Chapter 16
Magnetic Micro-/Nanopropellers for Biomedicine

Tian Qiu, Moonkwang Jeong, Rahul Goyal, Vincent M. Kadiri, Johannes Sachs, and Peer Fischer

16.1 Introduction

The motion of micro- and nano-objects in a fluid is, in the most general case, described by the Navier-Stokes equation. However, biomedical applications benefit from propellers that are so small that the mass (inertia) becomes negligible in fluid media. In this case, the Navier-Stokes equation can be approximated with the Stokes equation, which is simpler and shows no explicit time dependence. Therefore, the propulsion behavior of externally powered micro- and nanopropellers, which are proposed to perform biomedical tasks such as targeted drug delivery or minimally invasive surgery in fluids and soft tissues, is determined by the Stokes equation. A common measure of the applicability of this approximation is the Reynolds (Re) number [1]:

$$\mathrm{Re} = \frac{\text{inertial forces}}{\text{viscous forces}} \tag{16.1}$$

T. Qiu · M. Jeong
Micro Nano and Molecular Systems Lab, Max Planck Institute for Intelligent Systems, Stuttgart, Germany

Cyber Valley Group Biomedical Microsystems, University of Stuttgart, Stuttgart, Germany

R. Goyal · V. M. Kadiri · J. Sachs
Micro Nano and Molecular Systems Lab, Max Planck Institute for Intelligent Systems, Stuttgart, Germany

P. Fischer (✉)
Micro Nano and Molecular Systems Lab, Max Planck Institute for Intelligent Systems, Stuttgart, Germany

Institute of Physical Chemistry, University of Stuttgart, Stuttgart, Germany
e-mail: fischer@is.mpg.de

Y. Sun et al. (eds.), *Field-Driven Micro and Nanorobots for Biology and Medicine*, https://doi.org/10.1007/978-3-030-80197-7_16

If the inertial forces are small, which is the case for microswimmers and nanorobots, viscous fluid forces are dominant. This is the regime of low Reynolds numbers (Re < 1), where reciprocal movements cannot propel a swimmer. This complicates the number of effective propulsion mechanisms at low Re, a fact that is captured by the "scallop theorem" of Purcell [2]. A scallop that opens and closes its arms periodically cannot swim. It does not matter how fast or slow the scallop opens or closes its arms, as at the end of the opening and closing cycle, which is reciprocal, it experiences no net displacement. Thus, in Newtonian (incompressible) fluids, like water or glycerol, biological and artificial microswimmers (that are not pulled by an external force or torque) require more sophisticated propulsion strategies.

One possibility to overcome the problem of time-reversibility is demonstrated by flagellated bacteria that spin their flagella in a corkscrew-like stroke in order to swim. Here the continuous rotation is non-reciprocal, because of the chiral symmetry of the flagella. The propeller effect describes the translation of a helix due to rotation-translation coupling [3]. It is an efficient method for propulsion especially for very small microswimmers. The handedness of the (chiral) corkscrew and its rotation sense fixes the direction of the movement, e.g., a right-handed screw moves forward upon a clockwise rotation and backwards upon a counter-clockwise rotation. In contrast, the left-handed mirror-image structure will translate in the opposite direction.

It is also possible to build artificial corkscrew-shaped propellers that mimic this propulsion strategy. These have been experimentally demonstrated by utilizing rigid micro-screws that where actuated by means of an external magnetic field that is rotating (Fig. 16.1) [4–6]. The rotation of the propeller by an external torque (as opposed to the inherent internal motion provided by the bacterium) is also advantageous for actuation. The slender body of the corkscrew means that the structure can be used to efficiently navigate complex biofluids. Rotating magnetic fields can also be more easily established over larger volumes and at greater distance than magnetic gradient fields. The latter can only be used to pull a magnetic object, whereas the unidirectional motion of a screw-propeller ensures high maneuverability and

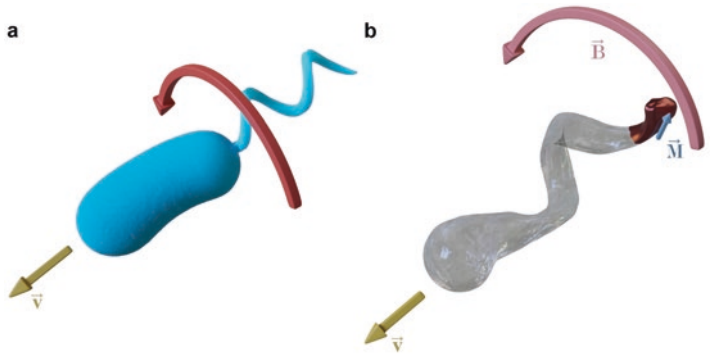

Fig. 16.1 Artificial micro-/nanopropellers (**b**) mimic bacteria flagella (**a**) to rotate and propel at small scale in fluids for biomedical applications

controllability, which is a highly desirable feature for externally powered biomedical devices.

In this book chapter, we review recent advances concerning artificial micro- and nanopropellers that are powered by magnetic fields and that can navigate through biological fluids and tissues for potential biomedical applications. Specifically, the chapter is organized as follows: In Sect. 16.2 we review the symmetry requirements for propulsion at low Re numbers by rotation-translation coupling; in Sect. 16.3 we describe the fabrication of micro-/nano-helices using physical vapor deposition; in Sect. 16.4 we review schemes to wirelessly actuate micro- and nanopropellers with magnetic fields. In Sect. 16.5 we discuss materials and, in particular, recent achievements in realizing propellers that are biocompatible, which is important for biomedical applications.

16.2 Theory of Micro-propulsion by Rotation-Translation Coupling

The propulsion force of the micro-/nanopropellers in fluids is generated by the coupling of the rotation to the translation of a helical shape. The rotation of the structures is generally driven by an external rotating magnetic field. We assume there is no field gradient and that no other external forces are present. The solution to the Stokes equation in low Re hydrodynamics reduces to two coupled equations [1]:

$$\begin{aligned} \boldsymbol{U} &= \boldsymbol{C}^{-1}\boldsymbol{L} \\ \boldsymbol{\Omega} &= \boldsymbol{B}^{-1}\boldsymbol{L} \end{aligned} \tag{16.2}$$

where $\boldsymbol{U}$ is the translational velocity vector and $\boldsymbol{\Omega}$ the rotational (angular) velocity of the object, whereas $\boldsymbol{L}$ is the torque exerted on the object by the external field. The coupling mobility tensor $\boldsymbol{C}$ and the rotation resistance tensor $\boldsymbol{B}$ relate the external torque to the objects' translational and rotational motion. Further, the equations show that, in general, the object's rotational motion is coupled to its translation, i.e., a translating body will always rotate and a rotating body will always translate, if the corresponding tensors are nonzero.

The exact form of the tensors $\boldsymbol{B}$ and $\boldsymbol{C}$ is determined by the geometry of the propellers' body, i.e., its symmetry. For example, a sphere, is an object with highest symmetry with three mutually perpendicular planes of mirror symmetry, has $\boldsymbol{C} = 0$ [1]. Consequently, a sphere cannot be propulsive by means of rotation-translation coupling at low Re. In contrast, a nonzero coupling tensor ($\boldsymbol{C} \neq 0$) is found for a chiral corkscrew shape. Thus, and because of the inspiration from biology, most experiments with artificial micro- and nanopropellers consider shapes with helical and thus chiral geometries in order to generate propulsion by means of an external rotating field. Chiral corkscrew shapes have been found to be optimal for propulsion [7]. It is generally assumed that chirality (handedness) is essential for efficient propulsion by means of an external rotating field and rotation-translation coupling.

This raises the question if chirality is strictly required for rotation-translation coupling or if a shape that is not chiral (achiral objects that possess mirror-image symmetry) can also translate when they are rotated by an applied magnetic field. This is not a purely academic question, as it is easier to synthesize or fabricate objects with high symmetry. Hence it is interesting to ask if such objects can also propel when magnetized and spun by a magnetic torque.

To shed light on this question, the fundamental symmetries that underlie rotation-translation coupling at low Re have recently been analyzed [8, 9]. Explicitly solving Eq. 16.2 for a magnetized and arbitrary shaped object [8, 9] that is subject to a rotating external field reveals that even objects that do not possess a chiral shape can propel at low Re. For instance, an achiral V-shaped body, which exhibits two mutually perpendicular planes of mirror symmetry, was shown to be able to propel under certain conditions. The V-shaped object was demonstrated to be propulsive as long as it does not rotate around one of its principal axes of rotation. However, theory and experiments proved that the orientation of the dipole moment with respect to the body of the V-shape plays a crucial role whether the V-shape can be propelled or not [9]. In the symmetry analysis, especially when determining if the object is chiral, it is essential that both the geometric shape and the object's magnetic dipole moment are considered [9]. If the symmetries of the whole object (shape and dipole) are considered, it is possible to correctly predict whether or not the object is propulsive and in this case if unidirectional or bidirectional propulsion will occur. The latter case means that the object has equal probability to move forward or backward, i.e., the rotation sense of the external field does not fix the propulsion direction. Note, however, that even the V-shape with its high geometrical symmetry can be designed to yield unidirectional propulsion if the V-shape is magnetized in a particular direction [9].

The mathematical definition of chirality is parity (spatial inversion), and hence, the V-shaped object's overall chirality is determined by executing the parity operator on both, the geometric shape and the dipole moment. Interestingly, in case of unidirectional propulsion, the object is necessarily chiral due to the orientation of the magnetic dipole moment it carries. On the other hand, one can design a magnetized chiral V-shaped object, which is non-propulsive upon rotation as is shown in Fig. 16.2. Therefore, chirality is certainly not a prerequisite for efficient propulsion via rotation-translation coupling, and in addition, parity alone does not fully explain the propulsion of such propellers. Instead, it becomes necessary to consider charge conjugation. Consequently, applying parity in conjunction with charge conjugation symmetry to a magnetized object is sufficient to fully predict whether the object will propel in a rotating magnetic field.

In practice, and in particular with a view of biomedical applications, magnetic fields applied to magnetized micro- and nanopropellers are used for externally driven propulsion, because it is easier to realize large torques. However, actuation of a V-shape by an external electric field is also possible and has recently been experimentally realized. Remarkably, because in this case the V-shape carries an electric dipole moment, and not a magnetic moment, its symmetry becomes achiral, and it therefore constitutes the first demonstration of an achiral propeller that propels by rotation-translation coupling at in a fluid at low Re [9].

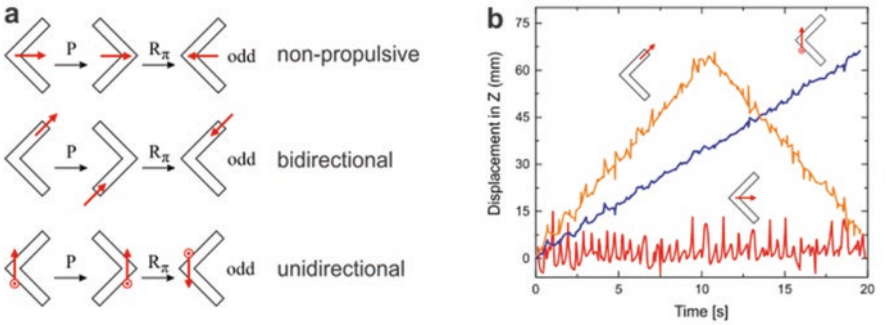

Fig. 16.2 Parity and charge conjugation symmetry need to be both taken into account to give a comprehensive prediction of low Re propulsion. (**a**) Three V-shaped objects that carry a magnetic dipole moment with different orientations (shown as the red arrows) with respect to the body shape. All three objects are parity-odd and therefore chiral but exhibit different propulsion gaits; (**b**) Experimental data show the propulsion gaits corresponding to the designs in a, including uni- and bidirectional, as well as a non-propulsive V-shaped object. (Reproduced with permission [61]. 2020, University of Stuttgart)

It should be mentioned that not only rotating but also precessing external fields, i.e., the external field vector rotates on a cone due to a superposition of an in-plane rotating field with a constant component orthogonal to it, can be used to propel highly symmetric V-shaped objects. In this case, also propellers, which are non-propulsive in a rotating field, can exhibit unidirectional motion [10]. Extending the types of applied magnetic fields from purely rotational to precessing fields and at the same time to consider additional geometrical shapes promises to extend the design space of propulsive micro- and nanorobots for biomedicine.

Irrespective of the body shape or its symmetry, the velocity of external field-driven propellers always depends on the external field's rotation speed [6, 8, 9]. Beyond a certain rotation frequency, at the step-out frequency, the micro- or nano-propellers can no longer follow the external field any more. Therefore, they will not maintain a constant angular synchronous velocity for frequencies larger than the step-out frequency. Instead, an asynchronous slip-motion will occur, and the propulsion velocity will drop to zero. The step-out frequency depends on several parameters, e.g. the strength of the magnetic dipole moment, the amplitude of the external magnetic field, and the viscosity of the fluid.

The discussion in this section starts with the governing Stokes equation, which does not have any explicit time dependence, and thus a reciprocal motion does not lead to a net translation in Newtonian fluids. However, most biofluids are non-Newtonian (e.g., the vitreous, mucus, blood, and so on), and in such fluids the time-reversibility problem can also be overcome by exploiting the time-dependent properties of the fluid itself, i.e., a scallop can even with reciprocal motion generate a net translation in non-Newtonian media. For this, it has to open and close its arms with varying speeds, as has been demonstrated with an artificial micro-scallop that was actuated with an external oscillating magnetic field [11]. Utilizing the biofluids' non-Newtonian rheology, i.e., its shear rate-dependent viscosity, allows the small

robot to propel with a reciprocal motion. This significantly simplifies the robot design and allows most actuators to be used for swimming in most biological fluids, even though they are not propulsive in Newtonian fluids (water) due to the scallop theorem. This may lead to new designs of simpler artificial microswimmers that are especially designed to operate in biological media and tissues.

16.3 Fabrication of Micro- and Nanopropellers by Glancing Angle Deposition (GLAD)

A few microfabrication techniques exist to fabricate micron-sized corkscrew shapes, but we focus here on the technique known as glancing angle deposition (GLAD). This technique can be used to fabricate the smallest propellers as well as the highest number of propellers, and that allows a large number of materials to be used including the strongest magnetic materials, which as we shall show are nevertheless biocompatible. The complex helix-shaped micro- and nanopropellers mentioned in the previous section were all fabricated using GLAD. It is a physical vapor deposition (PVD) method where a solid source material is heated in a crucible, either thermally or by an electron beam, under high vacuum conditions until it starts to melt and evaporate. Due to the low background pressure, the evaporant forms a directed flux and coats a surface (substrate). The substrate, on which the propeller structures grow, is tilted and held into this flux. Thus, the incident atoms and molecules adsorb on the surface of the substrate. The micro- and nanopropellers are not grown under normal incidence as is customary in PVD, but with oblique angle deposition (OAD), a technique where the evaporant and the substrate are intentionally tilted with respect to each other. Due to the tilt, the flux is shadowed, especially if there are any seed particles, and columnar structures will grow. The tilt-angle is commonly denoted as α, as shown in Fig. 16.3a. The GLAD technique adds another degree of freedom by rotating the substrate during deposition around the surface normal. The corresponding angle is denoted by ϕ. Those two parameters can be either constant or dynamically adjusted to grow complex and low-symmetry-shaped bodies on the micro- and nanoscale. Usually α is constant and if ϕ is constant too, a tilted column will form. If this process is repeated after the ϕ angle was changed by 180°, another column tilted in the opposite direction grows on top, and hence results in the V-shaped zig-zag structure as shown in Fig. 16.3b. Sometimes it is useful to have columnar structures that form columns perpendicular to the substrate. This is possible if a constant α angle and a continuous and fast ϕ rotation is used during the deposition process. An example of such pillar structures is shown in Fig. 16.3c. In case the ϕ angle is varied continuously but with a slow rotation speed, a helical corkscrew shape will form. Thus, the GLAD technique is useful for the fabrication of complex three-dimensional micro- and nanostructures, sometimes also denoted sculptured thin films (STF). During the deposition, multiple materials can be combined or deposited sequentially, which results in a large number of possible shapes

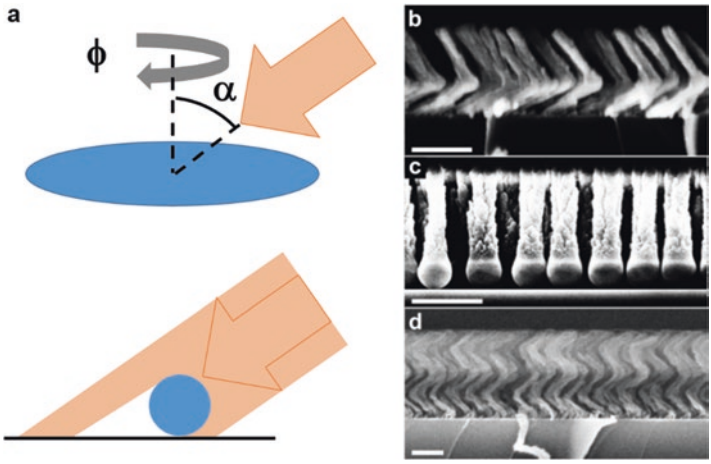

Fig. 16.3 Glancing angle deposition for the fabrication of micro-/nanopropellers. (**a**) Schematic visualization of the deposition process and the shadow effect. (**b**) SEM of nano-zigzags with one arm Ni and one arm SiO_2 grown on Au nanodots (scale bar 200 nm). (**c**) TiO_2 pillars grown perpendicular to the substrate on SiO_2 beads (scale bar 1 μm). (**d**) Chiral corkscrew-shaped SiO_2 structures grown on Au nanodots (scale bar 200 nm). ((**b**), (**c**), and (**d**) are reproduced with permission [61]. 2020, University of Stuttgart)

and structures. Typically 10^9–10^{10} structures grow on a cm^2 of substrate area. The entire growth process only takes a few hours.

To further facilitate the shadow-effect pre-patterned substrates are used, which already have well-structured nucleation seed patterns. A common procedure is to create a monolayer of closed-packed silica beads with sizes between 0.1 μm and 5 μm on a silicon substrate [12]. The seed particles can be deposited on an entire wafer using the Langmuir-Blodgett method [6]. For this purpose, nanoparticles, such as silica beads, are first gently pipetted onto a water surface and then transferred to the wafer by dip coating. The vertical columnar structures seen in Fig. 16.3c were grown on top of a monolayer of Langmuir-Blodgett-deposited SiO_2 beads. Another method for pre-patterning the GLAD substrate is to use Block-Copolymer-Micelle-Nanolithography [13], a method that coats a wafer with a (non-closed-packed) hexagonal monolayer of ~10 nm gold nanoparticles. This method has been used to pattern the substrate on which the zig-zags and helices in Fig. 16.3b, d were grown. The pre-patterning improves the quality of the structures, as it prevents the fusion of particles during the deposition. Depending on the materials that are used, it is sometimes also advantageous to actively cool the substrate during evaporation, which means the thermal energy of the incident atoms is reduced and hence their ability to diffuse on the substrate after their adsorption. This can be an important feature as the high surface mobility of the adatoms facilitates the growth of highly symmetric (e.g., spherical) shapes rather than complex structures, such as helices [14].

Another advantage of GLAD is the wide choice of possible evaporation materials as well as the ability to alloy several elements by simultaneous evaporation of two or more source materials. Micro- and nanopropellers typically comprise a magnetic head, grown with a fast ϕ rotation of, e.g., Co, Fe, or Ni (but also see Sect. 16.5 for a discussion of biocompatible materials), followed by a helical structure made out of an oxide such as SiO_2 [6]. After the GLAD process, the propellers are magnetized in a strong external magnetic field while still attached to the substrate. For further applications, the individual structures are then transferred into solution via ultrasonication to obtain colloidal suspensions of magnetic propellers.

16.4 Magnetic Actuation Systems

Micro-/nanopropellers cannot use traditional powering and actuation mechanisms as in large-scale robotics, such as on-board batteries or electromagnetic motors, due to their small size. Moreover, tethers for power transfer, such as wires or tubing, would restrict the locomotion of small-scale robots; thus untethered power transmission is needed for minimally invasive biomedical applications. Magnetic fields are commonly used in the medical field for imaging as well as for wireless actuation [15], due to its large biological tissue penetration depth, high controllability, and reliability. The magnetic fields can exert relatively large forces and/or torques on small-scale magnetic robots [16].

The magnetic torque $\boldsymbol{\tau}$, which is generated in a magnetic material is:

$$\boldsymbol{\tau} = \boldsymbol{m} \times \boldsymbol{B} \tag{16.3}$$

where $\boldsymbol{m}$ is the magnetic moment and $\boldsymbol{B}$ is the external magnetic field vector. The torque applied on the magnetic material/structure can cause translation, for instance, via rotation of a micropropeller [17] or can induce an angular displacement of a magnetic rod [18].

Magnetic fields have also been widely applied to the actuation of micro-/nanorobots for potential biomedical applications both in vitro and in vivo [19–21], i.e., steering a micro-guidewire by a magnetic field gradient [22], propelling micro-/nanopropellers in biological fluids by a rotating magnetic field [23–25], conducting micro-rheological tests [18], and steering chemically powered micro-/nano-motors in the intestine [26–28].

The generation and control of the magnetic field is achieved either by a specific configuration of permanent magnets or by controlling the electric currents in electromagnetic coils. A few examples of magnetic actuation systems are summarized in Table 16.1. In this section, we discuss some typical magnetic actuation systems. These systems are often customized, and the details depend on the particular application, i.e., the required field strength, the working volume, and the frequency range in case of an oscillating field. The design of the magnetic actuation system therefore needs to consider particular applications and operating conditions. Two main categories, i.e., permanent magnet systems and electromagnetic systems, are discussed

Table 16.1 Comparison of published magnetic actuation systems

Types	DOF[(a)]	Field strength [mT]	Rotating frequency [Hz]	Working volume [cm^3]	Size of the robot [μm]	Working media	No. of magnets/ coils	Size of each magnet/coil [mm]	Ref.
Permanent magnet systems	1	105	20	8	Φ10 × 250	Vitreous of porcine	4	30 × 30 × 30	[62]
	5	30	10	0.5	250	Silicone oil	8	25.4 × 25.4 × 25.4	[31]
	2	100	Manual rotation	–	Φ30	Dodecane	16 inside 8 outside	Φ34 × 19.5 octagon	[33]
Electromagnetic systems	3	10	>1 kHz	0.125	Φ0.5 × 2	Vitreous of porcine	6	Φ40 (inner), Φ70 (outer), 10 (height), largest coil	[63]
	–	Up to 400	100	~ 4000	20,000 In length	Pork fillet	18	~Φ350, ~Φ450	[38]
	5	50	–	4	2500 In length	Chick choriallantoic membrane	8	Φ62 × 210	[37]
	6	100	–	–	Φ1000 × 1000	Arteries of swine	Clinical MRI scanner		[22]

(a) Degree Of Freedom

Table 16.2 General comparison of magnetic actuation systems

Key parameters	Permanent magnet systems	Electromagnetic systems
Field strength	Strong	Weak
Working space	Large	Small
Controllability (on/off)	Low	High
Driving frequency	Low	High
Active cooling system	No	Yes
Mechanical motion, noise, and vibration	Yes	No
System total weight	Low	High
Cost	Low	High

in the following sections, respectively, and their advantages and disadvantages are compared in Table 16.2.

16.4.1 Permanent Magnet Actuation Systems

The basic concept of an actuation system based on permanent magnets is that several permanent magnets are distributed in space in a particular configuration to generate a superimposed magnetic field that is controllable in a defined volume. Compared to electromagnetic setups (Table 16.2), permanent magnet-based systems often offer higher field strength in a larger working volume. Moreover, permanent magnets do not require expensive ancillary equipment, such as electric amplifiers or active cooling systems. They are also less bulky, lighter, and generally cheaper. However, the trade-off is that the permanent magnet is always energized and that mechanical driving systems are required, in order to change the field amplitude or direction. Mechanically moving permanent magnets is also not suitable for high-frequency actuation.

Combining several permanent magnets that can be manipulated individually in their position and orientation provides a system with several degrees of freedom (DOF). For example, superimposing magnetic fields from a pair of magnets at an angle creates a small region of zero magnetic field strength, which can be used to push magnetic particles away from the permanent magnet [29].

To generate a time-varying magnetic field, a mechanical drive system is needed to rotate or translate the permanent magnets. As the permanent magnets cannot be "turned off" and since the magnetic attraction force between two magnets is inversely proportional to the distance square, the attractive force pulling a magnetic object toward the magnet can lead to very strong forces at short distance and can be a cause for safety concerns. A safer design does not rely on translation of magnets, but instead utilizes the rotation of the permanent magnets around a fixed support axis. Different approaches are listed in Table 16.1 and can be categorized according to three basic criteria:

1. The magnets are connected by a synchronizing mechanical drive mechanism (e.g., via a belt or gears) and are driven by one electrical motor (Fig. 16.4a) [18, 30]. Jeong et al. presented a magnetic actuation system using the synchronized rotation of four permanent magnets [18] (Fig. 16.4a). The magnets are firstly positioned in a desired direction and then connected using a timing belt-pulley to achieve a rotating magnetic field that is homogeneous at the center and that showed a strength of 105 mT. This system was designed for biomedical applications, with ample of space in between the magnets and access ports in all directions to accommodate medical imaging equipment, such as X-ray, ultrasound, and fluorescent imagers. These were used to localize the robots in the specimen. Although the system has only 1-DOF rotation, the addition of two sets of magnets provides two additional DOF, making the setup comparable to a 3-axis Helmholtz coil system.
2. Each magnet is individually driven and rotated by an electrical motor (Fig. 16.4b) [31, 32]. A permanent magnet system which has 5-DOF was reported by Ryan et al. using eight independent rotating magnets attached to eight servo motors. This system could generate a magnetic field of 30 mT and a magnetic gradient of 0.83 $T \bullet m^{-1}$ and no constraints on the direction of the magnetic fields [31]. This kind of system with multiple motors allows individual rotation of each magnet, which allows for the control of the magnetic gradient and the field direction [31, 32]. However, it requires several strong motors (that match the strong magnetic torque between the permanent magnets), and it requires a synchronized control of each of them.
3. The combination of a set of fixed magnets and a set of rotatable magnets (Fig. 16.4c) [33]. Baun et al. reported a system that is composed of an inner ring with 16 magnets and an outer ring with 8 magnets that can achieve a field strength of 100 mT and a gradient of 0.3 $T \bullet m^{-1}$ [33]. The magnets on the system are coaxially assembled along a specific direction to generate a dipolar magnetic field, a quadrupolar magnetic field, and the combination of both magnetic fields which defines the magnetic gradient to manipulate objects placed in the working volume. The movement direction is controlled by rotation of the outer ring (quadrupole). If particles are not placed in the center, they move slowly toward the rim due to the magnetic gradient.

16.4.2 Electromagnetic Actuation System

Many types of electromagnetic systems have been proposed and are commonly used to manipulate small-scale robots. Basically, magnetic fields are generated by controlling the electric current applied to a coil or to a pair of coils. One of the advantages of electromagnets is that the strength of the magnetic field is controllable even at high frequency.

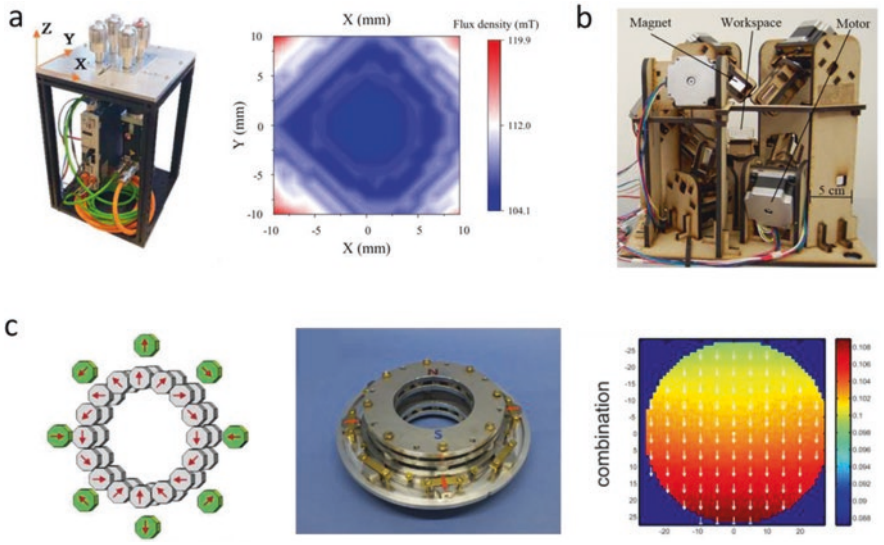

Fig. 16.4 Permanent magnet actuation systems. (**a**) Synchronized magnet rotating system; (**b**) Independent controllable magnet system; (**c**) Three cylinder Halbach system. (Reproduced with permission. (**a**) [18] 2019, IEEE; (**b**) [31] 2019, IEEE; (**c**) [33] 2017, Elsevier)

One of the commonly used types of electromagnetic actuation systems is a Helmholtz coil geometry. The Helmholtz coil is comprised of a set of identical coils aligned coaxially where the distance between the two coils equals the radius of coil. This particular configuration ensures a relatively homogeneous magnetic field in the central region between the two coils, which is beneficial for the study of micro-/nanopropellers that are actuated by a rotating magnetic field. This gradient-free system permits the study of magnetic torque-driven micro- and nanorobots. Assembling three pairs of (Helmholtz) coils (Fig. 16.5a) along three orthogonal directions can be used to generate relatively homogeneous fields that can point in any arbitrary direction. Wu et al. used a system of three pairs of coils that were arranged in an almost Helmholtz-like geometry to control the propulsion of helical magnetic micropropellers to move in the porcine vitreous to reach the optic disc region on the retina [25].

Electromagnetic actuation systems have also been widely used to generate gradient fields [23, 34–36]. For example, Kratochvil et al. demonstrated 5-DOF (3 translation, 2 rotation) electromagnetic actuation system, named OctoMag (Fig. 16.5c) [34]. This system consists of eight electromagnetic coils and generates magnetic field strength of 50 mT in a working space of 4 cm^3. The magnetic field strength was strengthened by soft magnetic cores inside the coils. The OctoMag successfully demonstrated that the robot's movement could be controlled in a fluidic tank, and it

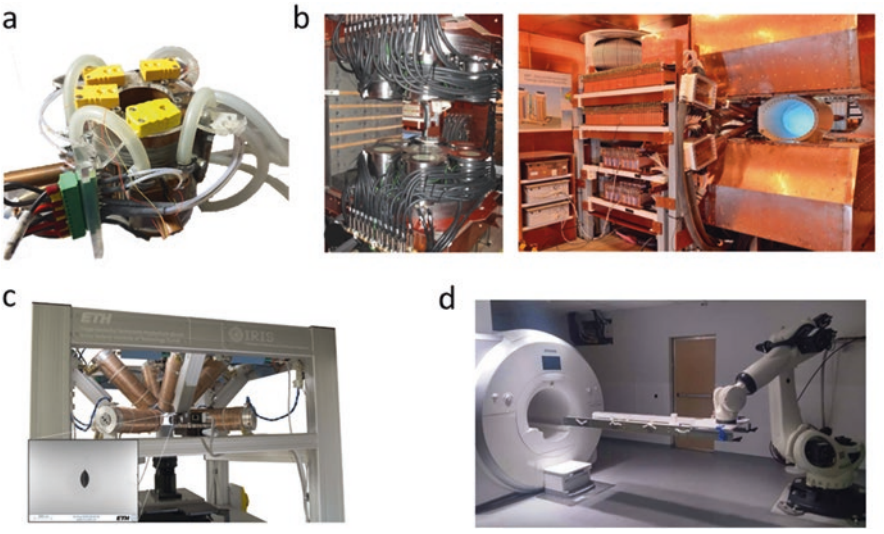

Fig. 16.5 Electromagnetic actuation systems. (**a**) A 3-axis Helmholtz coil with the cooling system; (**b**) A clinical-scale high-power system; (**c**) OctoMag system with 5-DOF; (**d**) The fringe field of an MRI scanner is used as the gradient field for magnetic manipulation. (Reproduced with permission. (**b**) [38] 2018, PLOS ONE; (**c**) [34] 2010, IEEE; (**d**) [22] 2019, Science Robotics)

also showed that it could be used to steer a needle tip to puncture tissue [37]. To extend these electromagnetic systems to accommodate a full human body, however, causes numerous engineering challenges. Rahmer et al. designed a clinical-scale magnetic field generator using 18 copper coils which have cylindrical soft magnetic iron-silicon cores to increase the field flux (Fig. 16.5b) [38]. The magnetic field strength from 30 to 90 mT at a frequency up to 10 Hz were applied for the experiment. The working space where the magnetic field is still homogeneous was reported to be spherical volume with a diameter of 200 mm. The resulting magnetic field was used to move a millimeter-scale helical robot to penetrate into a fillet of pork composed of muscle and connective tissue [38]. However, the system equipped with 100 kW cooling capacity uses more than 110 A per stack [38]. An alternate approach was presented by Azizi et al. who utilized the fringe fields of a superconducting magnetic resonance imaging (MRI) machine (Fig. 16.5c). A robotic arm was used to position a bed in the fringe field to navigate a guidewire in the blood vessels. The magnetic fringe field gradient (larger than 2 $T \bullet m^{-1}$) from the MRI scanner exerted a large pulling force to steer the tip of the micro-guidewire in the neck and brain arteries of a swine [22]. However, objects placed in the vicinity of an MRI magnet also compromise the quality of the field homogeneity necessary for nuclear magnetic imaging.

It is clear that electromagnetic actuation systems outperform permanent magnet systems in aspects of controllability and whenever time-varying fields are needed. They are in general also safer to operate. However, electromagnetic coils require cooling systems and expensive power supplies and are thus bulky and expensive. Regardless, whether electromagnetic or permanent magnets are used, the magnetic field strength always decays quickly over distance, which means it is difficult to realize high field strengths, which determines the magnetic driving force/torque on the robots, over a large volume (e.g., as is needed if it is to accommodate a human). Previous studies have shown that actuation based on homogeneous rotating magnetic fields scale better than gradient fields for a given distance [19]. Given the constraints in the magnet system, it is advantageous to optimize the micro-/nanopropeller design (helical geometry) and the magnetic materials, to increase the efficiency of converting the external driving magnetic field to actual locomotion inside biological fluids and tissues.

16.5 Biocompatible Magnetic Materials for Micro-/Nanorobots

Section 16.2 demonstrates the crucial role magnetic materials play in the maneuverability, reliability, and performance of magnetic propellers. Yet, as is to be expected in such a relatively young field, the fabrication and types of materials used for different propellers vary widely. While some materials can simply be deposited in a physical vapor deposition (PVD) chamber (e.g., Ni), others require more complicated solution processing or annealing steps ($Zn_xFe_{3-x}O_4$) [39]. In recent years, the use of nanopropellers has progressed from the first proof-of-concepts studies [4, 5] to the propulsion through biological media [24, 25, 40] as well as biomedical applications [41, 42]. This led to a closer inspection of the materials used in micro-/nanorobots [39, 43].

The following section will provide a few criteria which are helpful in evaluating the properties of magnetic materials and to judge their suitability toward specific, especially biomedical, applications. An overview of commonly used materials is provided. FePt in the $L1_0$ phase is identified as a particularly promising material for biomedical micro-/nanodevices.

16.5.1 Criteria for Magnetic Materials

Biocompatibility

Biocompatibility describes the absence of adverse biological effects (death, toxicity, oxidative stress) caused by the presence of a certain chemical or nanostructure. Determining cell viability is a common cell culture technique that can easily be

adopted for a rapid in vitro measure of biocompatibility. There are many types of ready-to-use commercial cell death assays. These are typically simple colorimetric assays, which are, for instance, based on calcein AM, a cell membrane permeable compound that is metabolized into a dye by live cells, and the ethidium homodimer-1, a membrane impermeable dye that only penetrates dead cells [44]. This in turn means that these dyes provide characteristic fluorescent readouts for dead versus live cells and hence biocompatibility that can be analyzed in a fluorescence microscope or via flow cytometry measurements. Assays like these can readily be performed in vitro with low cost. Compared to cell death assays, in vivo toxicity tests are as complicated, as they are varied due to the often complex interrelations between different cell types and organs. Regardless, in vivo biocompatibility testing is ultimately required for biomedical micro-/nanorobots to ascertain their long-term pharmacokinetics [42].

Magnetic Properties: Coercivity

The coercivity H_C describes the magnetic field necessary to re-magnetize a ferromagnetic material. The working principle of helical nanorobots, as depicted in Fig. 16.1, however, relies on reorienting a magnetized section thereby transferring torque τ – without re-magnetizing the robot. For this, low ~2 to 100 mT rotating fields are used. Soft magnetic materials that have coercivities in the ~mT range are thus unsuitable as magnetic materials for nanopropellers. This, conversely, justifies the use of high coercivity (~T) materials – hard magnets – in nanopropeller applications, to avoid re-magnetization while allowing for the application of high magnetic fields.

Magnetic Properties: Remanence

The magnetic remanence M_R describes the residual magnetization in a ferromagnetic material in the absence of an external magnetic field. As Eq. 16.3 illustrates, the magnetic moment of a propeller determines the torque that can be applied to the robot. While keeping the driving magnetic field strength the same, a higher magnetic remanence allows for a higher torque, or inversely a smaller magnetic field strength B can achieve the same torque. The former could lead to higher propulsion velocities and the latter to a simplification of the magnetic setup.

Biodegradability

The biodegradability characterizes a materials' property to be digested via biological processes or decomposition in biological media such as blood or cell media. Biodegradation is a common feature of many macroscopic biomedical tools such as degradable sutures made from polylactic acid (PLA) and/or polyglycolic acid [45].

A major advantage of magnetic materials based on iron, for instance, is that they decompose easily inside the body. Their biocompatibility and rapid clearance are two major reasons why iron oxides have enjoyed increased popularity over the last years [46]. However, not every biodegradable material is necessarily biocompatible. In the case of nickel or cobalt, the products of the metals' dissociation are highly toxic toward cellular functions, making these materials rather undesirable for biomedical applications [47, 48].

The biodegradability of an entire microswimmer has been realized in coating helically shaped microorganisms (Spirulina) with biodegradable iron oxide nanoparticles [49–51]. Similarly, biodegradable polymers have been used to fabricate iron-oxide-containing artificial soft microswimmers by a number of methods [51–54]. The difficulty in all of these studies is that the magnetic loading is limited and the magnetic strength of the nanoparticles is also low, which results in weak magnetic moments and thus small torques. In contrast, FePt is a harder magnet with a far higher magnetization [43].

3D Nanostructuring

Section 16.2 introduces GLAD as a promising method of generating three-dimensional nanoswimmers. As discussed in the previous subsection, other methods such as 2-Photon polymerization are also capable of producing similar, if bigger, structures. The method of fabrication limits which materials can be used. For instance, the hard magnet NdFeB cannot be evaporated using an electron beam or thermal evaporation making it unsuitable for fabrication via GLAD. 2-Photon polymerization, while suitable for the fabrication of some biodegradable polymeric propellers, can only accommodate a relatively small loading of magnetic powders, such as FeO_x nanoparticles. Two photon polymerization cannot process more favorable metals with high magnetic remanence and coercivity. These typically have to be added in a subsequent processing step [55]. Direct incorporation of strong biocompatible magnetic materials is, however, possible with GLAD.

16.5.2 Magnetic Materials for Biomedical Applications

Nickel is cheap and has excellent deposition characteristics in PVD and has thus in the past been a material of choice for many early nanoswimmer applications [25, 55]. However, similarly to cobalt, it is not ideal for biomedical applications since it shows toxicity and is chemically unstable in biological media [48].

Iron, on the other hand, is similarly inexpensive and can also be nanostructured via GLAD [25]. Its corrosion and degradation products are biocompatible and iron typically exhibits a high saturation magnetization of 1.6 T. The remanent magnetization of pure iron is usually less impressive at the nanoscale (40 emu/cm^3), and crucially iron's coercive field of ~0.2 mT is low when compared to other hard

magnets like NdFeB's 1.2 T [56, 57]. Iron oxides are typically soft magnets and are thus not ideal materials in order to realize large forces and torques. Additionally, FeO_x species are difficult to nanostructure via PVD since carefully controlled post-processing steps are usually required to obtain the correct phase [58].

Combinations of multiple magnetic materials are also possible, at the expense of a more involved fabrication process, as demonstrated by Venugopalan et al. Here Fe is first deposited via GLAD or PVD, and solution processed annealed zinc ferrite coatings are subsequently incorporated. This process yields multimodal non-agglomerating nanopropellers that could double as magnetic hyperthermia agents [39].

Finally, NdFeB is probably one of the most widely used hard magnets. Since NdFeB is not stable in moisture, it typically has to be coated with a protective layer. In addition, NdFeB cannot easily be nanostructured using physical vapor deposition. However, there is an attractive processable, biocompatible hard magnet that is suitable for nanopropeller fabrication: iron platinum (FePt).

FePt a Strong Magnetic Material for Nanodevices

The $L1_0$ phase of iron platinum has recently come into focus as a promising material for the construction of hard magnetic nanodevices due to a number of advantages over NdFeB [59]. $L1_0$ describes the face-centered tetragonal phase of a ~50:50 iron/platinum alloy where iron and platinum positions are arranged in an alternating ABA fashion (Fig. 16.6 center) as opposed to a face-centered cubic phase. FePt has the highest recorded magnetic energy products of up to ~70 MGOe – the maximum magnetic energy storable in a material – and coercivities of up to 7 T that easily rival those of other conventional, typically Nd- or Sm-based hard magnets [59]. What makes this comparison especially interesting is the fact that FePt is completely rare-earth free. Due to the addition of the platinum and its effect on the iron's electronic configuration, FePt also exhibits a significantly higher remanence than pure iron, despite exhibiting a lower saturation magnetization of 3.1 μ_B (2.7 μB from Fe and 0.4 μ_B from Pt) [59]. While the merits of iron as a material for biomedical applications were already discussed, there is also precedence of platinum being used in this capacity. In addition, FePt can be processed without the need for inert gases, and it is unreactive and thus does not need to be coated with a protective layer [43, 59]. FePt is thus uniquely positioned to be a next-generation magnetic material for micro- and nanorobotic devices. L10 FePt nanoparticles smaller than 10 nanometers are considered as superparamagnetic contrast agents for MRI. It is not cytotoxic and is therefore a prime candidate for applications in biomedical nano- and microdevices that can leverage these hard magnets' unique combination of easy nanostructuring, biocompatibility, and high magnetic moments [60].

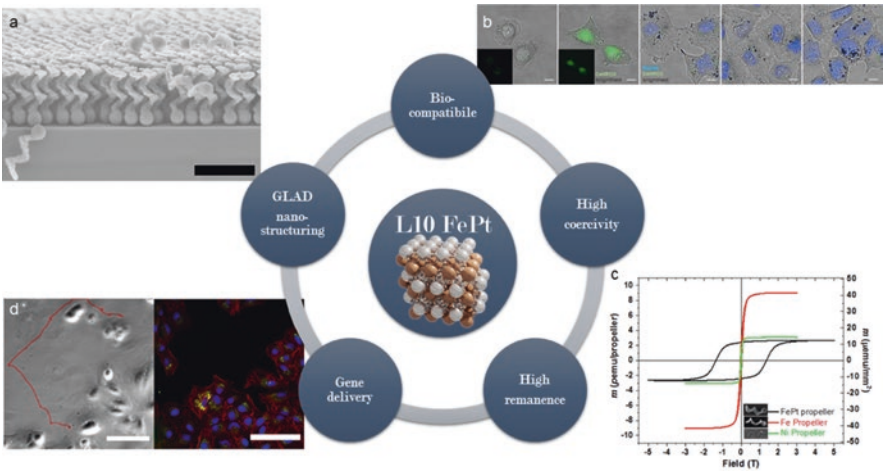

Fig. 16.6 $L1_0$ FePt (crystal structure in center) as a novel material for biomedical microswimmers. (**a**) The material can be 3D nanostructured via glancing angle deposition; (**b**) It is biocompatible (pictured are the results of a CellROX assay for reactive oxygen species.) and (**c**) It exhibits higher magnetic coercivity and remanence than previous materials Ni and Fe. (**d**) FePt-based microswimmers enable targeted active gene delivery in A549 cells. (Reproduced with permission [43]. 2020, Wiley VCH)

Fabrication and Characterization of FePt Nanopropellers

Using GLAD, nanopropellers that use FePt instead of the standard Ni or Fe can be fabricated via a co-deposition of iron and platinum followed by an annealing step at 680 °C to obtain the correct phase, fct $L1_0$. This phase transition can be observed both via XRD and SQUID magnetometry. The latter further reveals that $L1_0$ FePt as used in this shape exhibits a magnetic remanence of 333 emu/cm^3, which rivals that of microstructured NdFeB (400 emu/cm^3). Compared to Fe-based propellers of similar geometry, this is an eightfold increase in magnetic remanence [43].

Table 16.3 offers an overview of how nanostructured $L1_0$ FePt compares to other magnetic materials. The increased magnetic moments are also reflected in the maximum propulsion speeds for these propellers which reach up to 13 body lengths per second. Microswimmers' typical propulsion behavior increasing speeds for higher magnetic fields and frequencies is observed up to the respective step-out frequencies, where the propeller cannot follow the magnetic field.

Biocompatibility Tests and Gene Delivery

Despite both major components in the microswimmers (FePt and SiO_2) having individually been deemed biocompatible, it is important to note that their combination in the form of the microswimmer also shows no detectable toxicity. Upon

Table 16.3 Comparison of magnetic materials for micro-/nanopropellers

Material	Biocompatibility	Coercivity [T]	Magnetic remanence [emu/cm^3]	3D nanostructuring
Ni	No [47, 48]	0.01 [43]	11 [43]	PVD [41, 63]
Co	No [47, 48]	0.09 [64]	0.2 [65]	PVD [66]
Fe	Yes (concentration-dependent) [67]	0.028[43]	40 [43]	PVD [63]
FePt (680 °C)	Yes [43, 60]	1.3276 [43]	333 [43]	PVD [43]
NdFeB	–	1.2 (bulk) [57]	400 [43]	–
Fe_3O_4	Yes [46]	~0 [68]	~0 [68]	2-Photon-polymerization [52, 53]

incubation with multiple cell lines (HEK and A549), both the cell viability and reactive oxygen species (ROS) assays confirmed that the FePt nanopropeller is fully biocompatible [43].

This in turn allowed for their biomedical application to deliver green fluorescent protein (GFP) encoding plasmids into A549 cells. FePt microswimmers enabled both the passive transport of the plasmids into the cell's cytoplasm, which after an incubation time of 24 h started expressing GFP, and the active, i.e., targeted delivery.

16.6 Conclusion

In this chapter, we summarize some of the recent advances of magnetically driven micro-/nanopropellers for biomedical applications. We emphasize the challenges and new developments in the geometrical design, nano-fabrication, wireless actuation, and the choice of biocompatible materials for these small-scale robots. Recent advances have focused on motility studies in organ models in vitro or in ex vivo animal organs. The next step is to test these micro-/nanorobotic systems in vivo and to demonstrate a useful biomedical application. The constraints given by the relatively low torques that can be realized in laboratory magnetic systems calls for shape-optimized structures, with large magnetic moments that can also slip through the complex matrices found in real tissues and organs. Nanopropellers are thus promising for a truly minimally invasive nanomedicine of the future.

Acknowledgments The work is partially funded by the Max Planck Society. T.Q. and V.K. acknowledge financial support from the Vector Foundation. T.Q. and M.J. acknowledge the support by the Stuttgart Center for Simulation Science (SimTech).

Received: 30th of March 2021
Revised: 24th August 2021

References

1. Happel, J., & Brenner, H. (1981). *Low Reynolds number hydrodynamics* (Vol. 1). Springer Netherlands.
2. Purcell, E. M. (1977, January). Life at low Reynolds number. *American Journal of Physics, 45*(1), 3. https://doi.org/10.1119/1.10903
3. Baranova, N. B., & Zel'dovich, B. Y. (1978, August). Separation of mirror isomeric molecules by radio-frequency electric field of rotating polarization. *Chemical Physics Letters, 57*(3), 435–437. https://doi.org/10.1016/0009-2614(78)85543-2
4. Ghosh, A., & Fischer, P. (2009, June). Controlled propulsion of artificial magnetic nanostructured propellers. *Nano Letters, 9*(6), 2243–2245. https://doi.org/10.1021/nl900186w
5. Zhang, L., Abbott, J. J., Dong, L., Kratochvil, B. E., Bell, D., & Nelson, B. J. (2009, February). Artificial bacterial flagella: Fabrication and magnetic control. *Applied Physics Letters, 94*(6), 064107. https://doi.org/10.1063/1.3079655
6. Schamel, D., Pfeifer, M., Gibbs, J. G., Miksch, B., Mark, A. G., & Fischer, P. (2013, August). Chiral colloidal molecules and observation of the propeller effect terms of use. *Journal of the American Chemical Society, 135*(33), 12353–12359. https://doi.org/10.1021/ja405705x
7. Keaveny, E. E., Walker, S. W., & Shelley, M. J. (2013, February). Optimization of chiral structures for microscale propulsion. *Nano Letters, 13*(2), 531–537. https://doi.org/10.1021/nl3040477
8. Morozov, K. I., Mirzae, Y., Kenneth, O., & Leshansky, A. M. (2017, April). Dynamics of arbitrary shaped propellers driven by a rotating magnetic field. *Physical Review Fluids, 2*(4). https://doi.org/10.1103/PhysRevFluids.2.044202
9. Sachs, J., et al. (2018, December). Role of symmetry in driven propulsion at low Reynolds number. *Physical Review E, 98*(6). https://doi.org/10.1103/PhysRevE.98.063105
10. Cohen, K. J., Rubinstein, B. Y., Kenneth, O., & Leshansky, A. M. (2019, July). Unidirectional propulsion of planar magnetic nanomachines. *Physical Review Applied, 12*(1), 014025. https://doi.org/10.1103/PhysRevApplied.12.014025
11. Qiu, T., et al. (2014). Swimming by reciprocal motion at low Reynolds number. *Nature Communications, 5*. https://doi.org/10.1038/ncomms6119
12. Zhou, C. M., & Gall, D. (2006). The structure of Ta nanopillars grown by glancing angle deposition. *Thin Solid Films, 515*(3), 1223–1227. https://doi.org/10.1016/j.tsf.2006.07.136
13. Glass, R., Möller, M., & Spatz, J. P. (Oct. 2003). Block copolymer micelle nanolithography. *Nanotechnology, 14*(10), 1153–1160. https://doi.org/10.1088/0957-4484/14/10/314
14. Mark, A. G., Gibbs, J. G., Lee, T. C., & Fischer, P. (2013). Hybrid nanocolloids with programmed three-dimensional shape and material composition. *Nature Materials, 12*(9), 802–807. https://doi.org/10.1038/nmat3685
15. Sliker, L., Ciuti, G., Rentschler, M., & Menciassi, A. (2015, November 2). Magnetically driven medical devices: A review. *Expert Review of Medical Devices, 12*(6), 737–752. Taylor and Francis Ltd. https://doi.org/10.1586/17434440.2015.1080120
16. Li, D., et al. (2019). *Soft phantom for the training of renal calculi diagnostics and lithotripsy*. https://doi.org/10.1109/EMBC.2019.8856426
17. Li, D., Jeong, M., Oren, E., Yu, T., & Qiu, T. (2019, October). A helical microrobot with an optimized propeller-shape for propulsion in viscoelastic biological media. *Robotics, 8*(4), 87. https://doi.org/10.3390/robotics8040087
18. Jeong, M., Choi, E., Li, D., Palagi, S., Fischer, P., & Qiu, T. (2019, July). *A magnetic actuation system for the active microrheology in soft biomaterials*. https://doi.org/10.1109/MARSS.2019.8860985
19. Nelson, B. J., Kaliakatsos, I. K., & Abbott, J. J. (2010, July). Microrobots for minimally invasive medicine. *Annual Review of Biomedical Engineering, 12*(1), 55–85. https://doi.org/10.1146/annurev-bioeng-010510-103409
20. Fischer, P., & Ghosh, A. (2011, February 10). Magnetically actuated propulsion at low Reynolds numbers: Towards nanoscale control. *Nanoscale, 3*(2), 557–563. The Royal Society of Chemistry. https://doi.org/10.1039/c0nr00566e.

21. Nacev, A., et al. (2012). Towards control of magnetic fluids in patients: Directing therapeutic nanoparticles to disease locations. *IEEE Control Systems, 32*(3), 32–74. https://doi.org/10.1109/MCS.2012.2189052
22. Azizi, A., Tremblay, C. C., Gagné, K., & Martel, S. (2019, November). Using the fringe field of a clinical MRI scanner enables robotic navigation of tethered instruments in deeper vascular regions. *Science Robotics, 4*(36), 7342. https://doi.org/10.1126/scirobotics.aax7342
23. Qiu, T., Schamel, D., Mark, A. G., & Fischer, P. (2014, September). Active microrheology of the vitreous of the eye applied to nanorobot propulsion. In *Proceedings – IEEE international conference on robotics and automation* (pp. 3801–3806). https://doi.org/10.1109/ICRA.2014.6907410
24. Walker, D., Käsdorf, B. T., Jeong, H. H., Lieleg, O., & Fischer, P. (2015, December). Biomolecules: Enzymatically active biomimetic micropropellers for the penetration of mucin gels. *Science Advances, 1*(11), e1500501. https://doi.org/10.1126/sciadv.1500501
25. Wu, Z., et al. (2018, November). A swarm of slippery micropropellers penetrates the vitreous body of the eye. *Science Advances, 4*(11), eaat4388. https://doi.org/10.1126/sciadv.aat4388
26. Li, J., et al. (2016, October). Enteric micromotor can selectively position and spontaneously propel in the gastrointestinal tract. *ACS Nano, 10*(10), 9536–9542. https://doi.org/10.1021/acsnano.6b04795
27. De Ávila, B. E. F., et al. (2017, December). Micromotor-enabled active drug delivery for in vivo treatment of stomach infection. *Nature Communications, 8*(1), 1–9. https://doi.org/10.1038/s41467-017-00309-w
28. Wu, Z., et al. (2019, July). A microrobotic system guided by photoacoustic computed tomography for targeted navigation in intestines in vivo. *Science Robotics, 4*(32). https://doi.org/10.1126/scirobotics.aax0613
29. Shapiro, B., Dormer, K., & Rutel, I. B. (2010). A two-magnet system to push therapeutic nanoparticles. *AIP Conference Proceedings, 1311*(1), 77–88. https://doi.org/10.1063/1.3530064
30. Zhang, W., Meng, Y., & Huang, P. (2008, October). A novel method of arraying permanent magnets circumferentially to generate a rotation magnetic field. *IEEE Transactions on Magnetics, 44*(10), 2367–2372. https://doi.org/10.1109/TMAG.2008.2002505
31. Ryan, P., & Diller, E. (2016, June). Five-degree-of-freedom magnetic control of microrobots using rotating permanent magnets. In *Proceedings – IEEE international conference on robotics and automation* (Vol. 2016-June, pp. 1731–1736). https://doi.org/10.1109/ICRA.2016.7487317
32. Qiu, T., Palagi, S., Sachs, J., & Fischer, P. (2018, September). Soft miniaturized linear actuators wirelessly powered by rotating permanent magnets. In *Proceedings – IEEE international conference on robotics and automation* (pp. 3595–3600). https://doi.org/10.1109/ICRA.2018.8461145
33. Baun, O., & Blümler, P. (2017, October). Permanent magnet system to guide superparamagnetic particles. *Journal of Magnetism and Magnetic Materials, 439*, 294–304. https://doi.org/10.1016/j.jmmm.2017.05.001
34. Kummer, M. P., Abbott, J. J., Kratochvil, B. E., Borer, R., Sengul, A., & Nelson, B. J. (2010). OctoMag: An electromagnetic system for 5-DOF wireless micromanipulation. In *Proceedings – IEEE international conference on robotics and automation* (pp. 1610–1616). https://doi.org/10.1109/ROBOT.2010.5509241
35. Tasoglu, S., Diller, E., Guven, S., Sitti, M., & Demirci, U. (2014, January). Untethered microrobotic coding of three-dimensional material composition. *Nature Communications, 5*(1), 1–9. https://doi.org/10.1038/ncomms4124
36. Wang, X., et al. (2018, February). A three-dimensional magnetic Tweezer system for Intraembryonic navigation and measurement. *IEEE Transactions on Robotics, 34*(1), 240–247. https://doi.org/10.1109/TRO.2017.2765673
37. Kratochvil, B. E., Kummer, M. P., Abbott, J. J., Borer, R., Ergeneman, O., & Nelson, B. J. (2010). OctoMag: An electromagnetic system for 5-DOF wireless micromanipulation. In *Proceedings –IEEE international conference on robotics and automation* (pp. 1080–1081). https://doi.org/10.1109/ROBOT.2010.5509857

38. Rahmer, J., Stehning, C., & Gleich, B. (2018, March). Remote magnetic actuation using a clinical scale system. *PLoS One, 13*(3), e0193546. https://doi.org/10.1371/journal.pone.0193546
39. Venugopalan, P. L., Jain, S., Shivashankar, S., & Ghosh, A. (2018, February). Single coating of zinc ferrite renders magnetic nanomotors therapeutic and stable against agglomeration. *Nanoscale, 10*(5), 2327–2332. https://doi.org/10.1039/c7nr08291f
40. Pal, M., et al. (2018, May). Maneuverability of magnetic nanomotors inside living cells. *Advanced Materials, 30*(22), 1800429. https://doi.org/10.1002/adma.201800429
41. Mhanna, R., et al. (2014, May). Artificial bacterial flagella for remote-controlled targeted single-cell drug delivery. *Small, 10*(10), 1953–1957. https://doi.org/10.1002/smll.201303538
42. Venugopalan, P. L., Esteban-Fernández De Ávila, B., Pal, M., Ghosh, A., & Wang, J. (2020, August 25). Fantastic voyage of nanomotors into the cell. *ACS Nano, 14*(8), 9423–9439. American Chemical Society. https://doi.org/10.1021/acsnano.0c05217
43. Kadiri, V. M., et al. (2020, June). Biocompatible magnetic micro- and nanodevices: fabrication of FePt nanopropellers and cell transfection. *Advanced Materials, 32*(25), 2001114. https://doi.org/10.1002/adma.202001114
44. Stoddart, M. J. (2011). Cell viability assays: Introduction. *Methods in Molecular Biology (Clifton, N.J.), 740*. Humana Press, 1–6. https://doi.org/10.1007/978-1-61779-108-6_1
45. Kopeček, J., & Ulbrich, K. (1983, January 1). Biodegradation of biomedical polymers. *Progress in Polymer Science, 9*(1), 1–58. Pergamon. https://doi.org/10.1016/0079-6700(83)90005-9
46. Jain, T. K., Reddy, M. K., Morales, M. A., Leslie-Pelecky, D. L., & Labhasetwar, V. (2008, March). Biodistribution, clearance, and biocompatibility of iron oxide magnetic nanoparticles in rats. *Molecular Pharmaceutics, 5*(2), 316–327. https://doi.org/10.1021/mp7001285
47. Griffith, W. H., Pavcek, P. L., & Mulford, D. J. (1942). The relation of the sulphur amino acids to the toxicity of cobalt and nickel in the rat. *The Journal of Nutrition, 23*(6), 603–612. https://doi.org/10.1093/jn/23.6.603
48. Ermolli, M., Menné, C., Pozzi, G., Serra, M. Á., & Clerici, L. A. (2001, February). Nickel, cobalt and chromium-induced cytotoxicity and intracellular accumulation in human hacat keratinocytes. *Toxicology, 159*(1–2), 23–31. https://doi.org/10.1016/S0300-483X(00)00373-5
49. Yan, X., et al. (2015, September). Magnetite nanostructured porous hollow helical microswimmers for targeted delivery. *Advanced Functional Materials, 25*(33), 5333–5342. https://doi.org/10.1002/adfm.201502248
50. Yan, X., et al. (2017, November). Multifunctional biohybrid magnetite microrobots for imaging-guided therapy. *Science Robotics, 2*(12), 22. https://doi.org/10.1126/scirobotics.aaq1155
51. Peters, C., Hoop, M., Pané, S., Nelson, B. J., & Hierold, C. (2016, January). Degradable magnetic composites for minimally invasive interventions: Device fabrication, targeted drug delivery, and cytotoxicity tests. *Advanced Materials, 28*(3), 533–538. https://doi.org/10.1002/adma.201503112
52. Bozuyuk, U., Yasa, O., Yasa, I. C., Ceylan, H., Kizilel, S., & Sitti, M. (2018, September). Light-triggered drug release from 3D-printed magnetic chitosan microswimmers. *ACS Nano, 12*(9), 9617–9625. https://doi.org/10.1021/acsnano.8b05997
53. Wang, X., et al. (2018, November). 3D printed enzymatically biodegradable soft helical microswimmers. *Advanced Functional Materials, 28*(45), 1804107. https://doi.org/10.1002/adfm.201804107
54. Ceylan, H., Yasa, I. C., Yasa, O., Tabak, A. F., Giltinan, J., & Sitti, M. (2019, March). 3D-printed biodegradable microswimmer for theranostic cargo delivery and release. *ACS Nano, 13*(3), 3353–3362. https://doi.org/10.1021/acsnano.8b09233
55. Qiu, F., Fujita, S., Mhanna, R., Zhang, L., Simona, B. R., & Nelson, B. J. (2015, January). Magnetic helical microswimmers functionalized with Lipoplexes for targeted gene delivery. *Advanced Functional Materials, 25*(11), 1666–1671. https://doi.org/10.1002/adfm.201403891
56. Thompson, S. P. (1896). *Dynamo-electric machinery: A manual for students of electrotechnics*. American Technical Book Company.

57. Fuerst, C. D., & Brewer, E. G. (1993, May). High-remanence rapidly solidified Nd-Fe-B: Die-upset magnets (invited). *Journal of Applied Physics, 73*(10), 5751–5756. https://doi.org/10.1063/1.353563
58. Zhao, B. et al. (2007). *Iron oxide(III) nanoparticles fabricated by electron beam irradiation method*.
59. Son, K., et al. (2019, August). Superior magnetic performance in FePt L10 nanomaterials. *Small, 15*(34), 1902353. https://doi.org/10.1002/smll.201902353
60. Shi, Y., Lin, M., Jiang, X., & Liang, S. (2015). Recent advances in FePt nanoparticles for biomedicine. *Journal of Nanomaterials, 2015*. Hindawi Limited. https://doi.org/10.1155/2015/467873
61. Sachs, J. (2020). *Motion, symmetry & spectroscopy of chiral nanostructures*. University of Stuttgart.
62. Jeong, M., Choi, E., Li, D., Palagi, S., Fischer, P., & Qiu, T. (2019). *A magnetic actuation system for the active microrheology in soft biomaterials*. https://doi.org/10.1109/MARSS.2019.8860985
63. Wu, Z., et al. (2018, November). A swarm of slippery micropropellers penetrates the vitreous body of the eye. *Science Advances, 4*(11), eaat4388. https://doi.org/10.1126/sciadv.aat4388
64. Luo, H., Wang, D., He, J., & Lu, Y. (2005, February). Magnetic cobalt nanowire thin films. *The Journal of Physical Chemistry. B, 109*(5), 1919–1922. https://doi.org/10.1021/jp045554t
65. Wang, W., Giltinan, J., Zakharchenko, S., & Sitti, M. (2017, May). Dynamic and programmable self-assembly of micro-rafts at the air-water interface. *Science Advances, 3*(5), e1602522. https://doi.org/10.1126/sciadv.1602522
66. Ghosh, A., & Fischer, P. Controlled propulsion of artificial magnetic nanostructured propellers. https://doi.org/10.1021/nl900186w
67. Zhu, S., et al. (2009, June). Biocompatibility of pure iron: In vitro assessment of degradation kinetics and cytotoxicity on endothelial cells. *Materials Science and Engineering: C, 29*(5), 1589–1592. https://doi.org/10.1016/j.msec.2008.12.019
68. Maldonado-Camargo, L., Unni, M., & Rinaldi, C. (2017). Magnetic characterization of iron oxide nanoparticles for biomedical applications. *Methods in Molecular Biology, 1570*., Humana Press Inc., 47–71.